REPORT DOCUMENTATION PAGE

Form Approved
OMB No. 0704-0188

1. AGENCY USE ONLY *(Leave blank)*	2. REPORT DATE	3. REPORT TYPE AND DATES COVERED
	12/[illegible]/97	Final Technical Report 10/1/93 - 3/31/97

4. TITLE AND SUBTITLE
Investigation of Turbulent Boundary Layers Subjected to Internally or Externally Imposed Time-Dependent Transverse Shears

5. FUNDING NUMBERS
G
N00014-94-0104

6. AUTHOR(S)
Hassan Nagib
Candace Wark
Ron Adrian

7. PERFORMING ORGANIZATION NAMES(S) AND ADDRESS(ES)
Illinois Institute of Technology
MMAE Dept.,
10 W. 32nd St.
Chicago, IL 60616

8. PERFORMING ORGANIZATION REPORT NUMBER

9. SPONSORING / MONITORING AGENCY NAMES(S) AND ADDRESS(ES)
Office of Naval Research
Ballston Tower One
800 North Quincy St.
Arlington, VA 22217-5660

10. SPONSORING / MONITORING AGENCY REPORT NUMBER

11. SUPPLEMENTARY NOTES

a. DISTRIBUTION / AVAILABILITY STATEMENT

DISTRIBUTION STATEMENT A
Approved for public release
Distribution Unlimited

19980120 193

13. ABSTRACT *(Maximum 200 words)*

Both experimental and modeling efforts are aimed at understanding the non-equilibrium effects introduced by a 2-D turbulent boundary layer suddenly subjected to transverse wall shear. A new turbulence model has been developed which can be used to predict the Reynolds stress development in 3-D shear flows. This θ-l model allows for a misalignment to occur between the stress and strain as observed in 3-D turbulent boundary layers. The misalignment is determined by accounting for the flow history through solving a transport equation (first derived by Bradshaw, 1971) for θ. Excellent agreement is observed for both mean profiles and Reynolds stress when compared with the experiments of Driver and Johnston (1990). For the experiments, a 36' long 18" diameter cylinder surface is used. One section of the model is designed to rotate about its axis; thereby, introducing non-equilibrium effects into the developing 2-D boundary layer. Stereoscopic PIV is being used to acquire all three components of the velocity in both the x-y and x-z planes. Comparison of the detailed experimental results with subsequent modifications of the modeling should result in improved non-equilibrium turbulence prediction capabilities.

14. SUBJECT TERMS	15. NUMBER OF PAGES
3-D turbulence models, Non-equilibrium turbulence, Particle Image Velocimetry, Stereo PIV	20
	16. PRICE CODE

17. SECURITY CLASSIFICATION OF REPORT	18. SECURITY CLASSIFICATION OF THIS PAGE	19. SECURITY CLASSIFICATION OF ABSTRACT	20. LIMITATION OF ABSTRACT
Unclassified	Unclassified	Unclassified	UL

Investigation of Turbulent Boundary Layers Subjected to Internally or Externally Imposed Time-Dependent Transverse Shear

Final Report
ONR N00014-94-1-0104

H. M. Naguib
A. M. Naguib
C. E. Wark
S. Kiwan
S. Gravante
M. Mazanac

Fluid Dynamics Research Center
Illinois Institute of Technology
Chicago, IL 60616

R. J. Adrian
Z.C. Liu
C.D. Meinhart

Department of Theoretical and Applied Mechanics
104 S. Wright Street
University of Illinois
Urbana, IL 61801

December 1997

Introduction

Turbulence models have been developed to predict various mean and turbulence quantities for a wide variety of two-dimensional flows despite the fact that many of the flows encountered in practice are three-dimensional in nature. However, unlike the two-dimensional case, three-dimensional turbulence models are rare. In many situations three-dimensionality, curvature, rotation, buoyancy, pressure variation, etc. introduce changes in the turbulence structure, the effects of which cannot be predicted by many of the two-dimensional turbulence models. Therefore, it becomes increasingly important to develop suitable closure models for adequate predictions of turbulence in such complex flows.

One limiting factor encountered in modeling three-dimensional flows is that there are few experiments with sufficient data to guide modeling efforts: Driver, D. M., and Johnston (1990) and Schwarz, W. R., and Bradshaw, P. (1994). Consequently, most turbulence models for three-dimensional flows tend to be a mathematical generalization of models developed for two-dimensional flows, that, in many cases do not account for the physics associated with the effects of three dimensionality.

Three-dimensional turbulent boundary layers are generally classified as shear-driven or pressure-driven. The cross flow in shear-driven three-dimensional turbulent boundary layers is generated from shearing forces (extra strain) applied to the fluid by a moving surface. Whereas, the cross flow in pressure-driven three-dimensional turbulent boundary layers is generated by the application of a cross-stream pressure gradient, which deflects the streamlines of the low momentum flow close to the surface more strongly than those near the freestream. It is observed experimentally that the presence of a cross flow introduces three-dimensional effects that alter the structure of the turbulence, its length scales, intensities, etc.

Shear-Driven three-dimensional turbulent boundary layer experiments typically follow the innovative experiment by Furuya et al. (1966). Those authors performed mean-velocity measurements in a three-dimensional boundary layer developing along a circular cylinder in which the cross flow was produced by a spinning cylinder, the axis of which was aligned with a uniform freestream. Using a similar experimental setup, Driver and Hebbar (1987) measured all six Reynolds stress components as well as the mean flow in the experimental rig of Higuchi and Rubesin (1979). Later, Driver and Johnston (1990) also made direct measurements of the skin friction and all six components of the Reynolds stress in the same flow. They studied the combined effect of applying streamwise pressure-gradient simultaneously with the shear forces generated from surface motion.

Three-dimensional turbulent boundary layer experiments have been reviewed by Johnston (1976), Fernholz and Vagt (1981), and Anderson and Eaton (1987). It should be pointed out that although many experiments dealing with three-dimensional turbulent boundary layers have been reported in the literature (for example, in 1976, Johnston cited more than

80 experiments), those experiments measuring multiple components of the Reynolds stress tensor will be most useful when developing turbulence models. In many cases, the measurements of the complete Reynolds stress tensor are omitted because of experimental difficulties; e.g., see Schwarz and Bradshaw (1994).

Most of the experiments on three-dimensional turbulent boundary layers have documented a misalignment in the development between the turbulent Reynolds stress field relative to the mean flow field. This misalignment leads to anisotropy in the eddy viscosity which in turn renders all modeling efforts based on the isotropic (scalar) eddy viscosity hypothesis unsuccessful in predicting three-dimensional boundary layers. Specifically, the isotropic models assume that the mean-strain and turbulent-stress fields are aligned. Unfortunately, there is no general agreement in the experiments, whether the turbulent stress field leads the mean-strain field or visa versa. The experiments of Lohmann (1976) and Driver and Johnston (1990), which are shear-driven three-dimensional turbulent boundary layers, show that the stress field lags the rate-of-strain field. Thus, this stress-strain misalignment is often referred to as the stress-lag phenomenon.

Allowing for this stress-strain misalignment has been difficult for models to predict. Unlike models for two-dimensional turbulent flows, three-dimensional turbulent models are rare. This is, in part, because there are few experiments with sufficient data to guide modeling efforts, as indicated by Driver and Johnston (1990) and Schwartz and Bradshaw (1994). Several recent reviews have continued to recognize the need for better turbulence modeling in three-dimensional turbulent boundary layers (cf., Purtell (1992)). Therefore, this investigation has both an experimental as well as a modeling effort.

The present experiments are aimed at providing a clean and controllable "canonical" non-equilibrium flow that can be conveniently incorporated into computational schemes ranging from direct numerical simulation to large eddy simulation and eddy viscosity modeling. An 18" diameter, 36' long test surface is used for the experiment. A two-dimensional turbulent boundary layer develops along the surface of the cylindrical model. One section of the model is designed to rotate about its axis; thereby, introducing non-equilibrium effects into the developing 2-D boundary layer. The flowfield is studied for the steady rotation case as well as the time-dependent case. The time-dependent transverse shear is important to identify the role played by the rate at which the non-equilibrium effects are introduced or removed from the flow. Ultimate prediction and control of wall-bounded turbulent flows in the presence of complex geometry's will require knowledge of the type of information that will be generated from this work.

Documentation of the non-equilibrium flow will be accomplished using stereo Particle Image Velocimetry (PIV). This will provide all three components of the velocity in the measurement plane (see Prasad and Adrian [1992]); thereby, providing the full Reynolds stress tensor.

Results

Documentation of Base Two-Dimensional Turbulent Boundary Layer

The streamwise mean and fluctuating velocity were measured at three axial locations along the 18-inch diameter, 36-foot long cylinder (provided by NASA Langley Research Center) in the NDF test section (Figure 1) to validate the condition of the "equilibrium" turbulent boundary layer. The measurements were obtained along the "stationary" cylinder, i.e. without rotation, over the Reynolds number range $7450<Re_\theta<23900$ and demonstrate that the characteristics of the existing 2-D turbulent boundary layer are in good agreement with the classical observations of boundary layer scaling. From these data, and the measurements of the free-stream uniformity and turbulence intensity in the test section, it was concluded that the overall condition of the flow meets or exceeds expectations.

With regards to the free-stream, the velocity can be adjusted to within 0.1 m/s of the desired value, and can be held to within ±0.1 m/s over several hours of data acquisition. Additionally, the chilled-water cooling system of the wind tunnel typically can maintain steady-state temperature to within 0.1 °C at all tested free-stream velocities, and can be held to within ±0.1 °C over several hours of data acquisition. The turbulence intensity was measured using a pair of 2.5 μm diameter hot-wires and was shown to be less than 0.05% for all tested free-stream velocities. The total sound pressure level varied from 91 dB at 16 m/s to 111 dB at 55 m/s and was generally less than 0.5% of the free-stream dynamic pressure, indicating a relatively quiet flow within the test section. Finally, the streamwise pressure gradient was manipulated by adjusting the test-section ceiling panels, and when set for zero pressure gradient, exhibited less than 0.5% streamwise deviation of the mean free-stream velocity over the entire length of the cylinder.

The boundary layer mean velocity uniformity was measured with a Pitot-static probe at 3 cm from the cylinder surface and 7 m downstream of the nose of the cylinder at 24 azimuthal locations. The standard deviation of the mean velocity in the azimuthal direction was about 3% which demonstrated a strongly two-dimensional, axisymmetric boundary layer.

A single-component hot-wire was used to measure the streamwise velocity in the turbulent boundary layer which exists on the cylinder. The resulting parameters for the boundary layer measurements are given in Table 1. Figure 2 shows the streamwise mean and rms velocity scaled on inner and outer variables over the range $7{,}450 < Re_\theta < 23{,}900$ for three different streamwise locations along the cylinder and free-stream velocity in the range $12.1 < U_\infty < 37.6$ m/sec. The friction velocity was calculated by the Clauser method, and the three streamwise measurement locations correspond to positions upstream, on, and downstream of the section which will rotate during the non-equilibrium experiments. These plots show that there is no observable streamwise dependence in the velocity profiles and that the data compare well with the established scaling behavior of the canonical flat-plate boundary layer (or axial cylinder boundary layer with small δ/r).

Examination of the velocity spectra from the cylinder in Figure 3 reveal the typical traits of streamwise spectra at $y^+ = 50$, $y^+ = 100$, $y/\theta = 1.13$; i.e. the equilibrium range of scales consisting of the -1 slope overlap region and the -5/3 slope inertial subrange. Although it is not imperative to the establishment of the condition of the boundary layer on the cylinder, it is interesting to note the bimodal energy distribution in the spectra of cylinder data at $y^+ = 50$ (see bottom, left hand graph in Figure 3). This peak, which has also been observed in flat plate measurements, further illustrates the importance of inner- and outer-scale interactions since a second, low-frequency peak (i.e. outer-region influence) might not have been expected to persist down to the edge of the buffer layer at $y^+ = 50$. For more details see Hites (1997).

The cylinder measurements confirm the behavior of the turbulent boundary layer in that the boundary layer displays excellent two dimensionality and good agreement with established boundary layer measurements when the adjustable ceiling is set for a zero pressure gradient condition in the test section. In particular, the overlap region of scales increases with increasing Reynolds number, the mean and rms collapse in the classical sense with inner and outer scaling, and the velocity spectra reveal the well-documented equilibrium range.

Table 1. Cylinder Boundary Layer Parameters

x (m)	U_∞ (m/s)	Re_θ	u_τ (m/s)	θ (cm)	δ^* (cm)	l^+
3.7 (x_1)	19.8	8590	0.74	0.65	0.86	24
3.7	28.0	11400	1.02	0.61	0.80	34
5.8 (x_2)	12.1	7450	0.46	0.91	1.19	15
5.8	29.6	17400	1.04	0.87	1.13	35
5.8	37.6	22500	1.29	0.86	1.12	43
7.4 (x_3)	18.7	14000	0.67	1.12	1.44	22
7.4	26.9	18800	0.94	1.04	1.33	31
7.4	35.3	23900	1.21	1.01	1.28	57

Design of Cylindrical Rotating Section

The original test surface was an 18" diameter 36' long cylindrical model constructed primarily of aluminum and graphite fiber composite. The model is comprised of a nose cone, four cylindrical tube sections, a cable support ring, an A-frame support and an aft cone (see Figure 1). To introduce non-equilibrium effects into the developing 2-D turbulent boundary layer, one of the four cylindrical tube sections was replaced with a cylindrical segment capable of rotating about its axis. A schematic of the rotating cylinder section is shown in Figure 4.

In designing the rotating segment, the weight was minimized by designing the section primarily out of fiber composites and using light weight air motors to power the rotation. The stiffness was maximized by designing the section as a large diameter structural tube over which concentric outer tubes were slid in place. The inner structural tube is composed of a high modulus graphite fiber composite; whereas, the outer tubes are composed of glass

fiber composite. This section is composed of three independently rotatable 20″ long fiber-composite sections allowing for flexibility in the introduction of the transverse shear.

A bearing-cooling system (BCS) has been designed and constructed to remove the heat that is generated at the bearing interface. This system consists of copper tubing running along the stainless steel segment of the rotating cylinder bearings through which cold water, extracted from the thermal storage system used to control the flow temperature in the NDF, will be used to remove the excess heat generated at the interface of the stainless steel and Teflon segments of the bearing. Recent experiments have shown that by removing the excess heat generated by frictional forces, the cylinder can be made to rotate at approximately 1,000 rpm or 30 m/s. This will allow the rotation speed to match the freestream speed for the Reynolds number range considered in this investigation (i.e. $W_{wall}/U_{\infty} = 1$).

Modeling of Three-Dimensional Turbulent Boundary Layer

Recently at IIT, a new turbulence model has been developed (Kiwan, 1995). The new model is referred to as the $\theta - l$ model. This model is of the anisotropic type, and therefore it can be used to predict the Reynolds stresses developed in three-dimensional shear flows. The $\theta - l$ model allows for a misalignment to occur between the stress and strain as observed in three-dimensional turbulent boundary layer flows. The misalignment is determined by accounting for the flow history through solving a transport equation (first derived by Bradshaw, 1971) for the ratio θ of the transverse to the axial Reynolds stress components ($\overline{vw}/\overline{uv}$). This $\theta - l$ model also makes use of the mixing length concept to model the streamwise Reynolds stress.

The $\theta - l$ model has been tested against the experiments of Driver and Johnston (1990) for a zero-pressure-gradient, three-dimensional, shear-driven turbulent boundary layer flow. In this experiment, the collateral flow of a turbulent boundary layer developing over a cylinder spinning about its axis, encounters a stationary segment of the cylinder. This sudden change in the boundary condition introduces a non-equilibrium effect into the flow. Figure 5 shows a comparison between the computational (using the $\theta - l$ model) and experimental values of the axial mean velocity profiles over the stationary segment of the cylinder. It can be seen that excellent agreement exists. Figure 6 shows a comparison between the experimental and the computational values of the axial Reynolds stresses at various downstream locations over the stationary segment. It is clear form this figure that the $\theta - l$ model not only qualitatively but also quantitatively predicts the experimental values of the axial Reynolds stress.

Finally, Figure 7 demonstrates that the $\theta - l$ model is able to predict the stress-strain misalignment phenomenon observed in the experimental data of Driver and Johnston (1990). In this figure, a plot of the numerical and experimental values of the stress and strain angles (Θ and Φ, respectively) are plotted. On the same figure, the stress angle (defined at the bottom of figure) predicted by the nonlinear $k - \varepsilon$ model of Speziale (solid

line) is shown. The Speziale (1987) model was not able to predict the stress-strain misalignment phenomenon.

STUDY OF TURBULENT BOUNDARY LAYER USING A STEREOSCOPIC PARTICLE IMAGE VELOCIMETER

A stereoscopic particle image velocimeter for the measurement of three-dimensional vectors on a planar domain has been developed for use in the studies of the non-equilibrium boundary layers. The camera is based on two high-resolution video cameras. This system provides several unique capabilities. Stereoscopic PIV corrects for perspective error as well as providing the out-of-plane component. Videographic recording increases the ease of use substantially by eliminating the necessity of registering photographic images. The present system has been used to measure thousands of frames in experiments that required only a few days to set up. In addition to the quantitative value of the out-of-plane component, it is found that having the complete three-dimensional vector also significantly improves the qualitative visualization of the flow. Although the video-based PIV system has less resolution than a photographic system, it is encouraging that it is still able to resolve many of the important features of the turbulent boundary layer that have only recently been discovered by photographic PIV. The results are very similar to those obtained by photographic PIV. Thus, while the video system clearly has a important role to play in the acquisition of three-dimensional data for analysis by statistical averaging, it also provides enough resolution to be of considerable value in visualizing the flow.

IIT has purchased a Nd:Yag Surelite II PIV laser system from Continuum. It is an integrated system containing two pulsed lasers (10 Hz) and the combining optics needed to overlap the beams. The lasers are capable of generating 300 mJ pulses which will be sufficient to provide the required depth of field for the stereo camera.

Seeding particles are an atomized mixture of 90% water and 10% polyethylene-glycol. Three to four TSI model 9306 6-jet atomizers which are capable of producing micron sized particles are used for this purpose. This system has also been used successfully in the Mark V. Morkovin facility at IIT on another ONR sponsored PIV investigation.

Initially, measurements are made in x-y and x-z planes where x, y, z are the streamwise, wall normal and spanwise coordinates, respectively. Due to the requirements of sheet width and thickness and the physical constraints present in the NDF, two sets of optics are required for the initial set of measurements. For measurements in the x-y plane the optics, shown in the top plot of Figure 8, consist of a 25.4 mm cylindrical lens and a 450 mm spherical lens which produces a 106 mm wide sheet. The sheet, located on the underside of the cylinder, can be focused to a minimum thickness of 0.5 mm for the non-rotating case (i.e. no out-of-plane component) or to a maximum thickness of 1.7 mm for the rotating case. The larger depth of field is required for the x-y plane when a transverse shear is applied since a significant mean velocity (W) normal to the light sheet is present. Shown in

the bottom plot of Figure 8 is the optics configuration for measurements in the x-z plane. The laser sheet is produced with a 80 mm cylindrical lens, two right angle prisms, and 1000 mm spherical lens. It is approximately 80 mm wide, 0.3 mm thick and located on the side of the cylinder. A thicker sheet is not required for the x-z plane since during rotation of the cylinder there is no significant out-of-plane velocity for this measurement.

Measurements in the x-y plane will be taken at four stations: 4.3 m, 5.2 m, 6.0 m, and 7.4 m downstream of the leading edge of the cylinder. These measurements will be taken in the equilibrium (non-rotating) turbulent boundary layer on the underside of the cylinder. The 4.3 m location is just upstream of the section of the test surface designed to rotate. The 5.2 m and 6.0 m positions are located on the surface of the section designed to rotate. Based on the θ-l modeling results of Kiwan (1995) these positions correspond to locations where the flow is three-dimensional and collateral respectively. The last measurement location of 7.4 m is downstream of the segment designed to rotate and the flow is expected to be three-dimensional again before becoming an equilibrium turbulent boundary layer. These measurements will be obtained over the range of Reynolds numbers of $4{,}000 < Re_\theta < 10{,}000$. They will provide an instantaneous description of the streamwise and wall-normal structure of the flow field in the two-dimensional turbulent boundary layer as a function of Reynolds number. A large number of realizations, on the order of 1,000, will be obtained for each Reynolds number at each station. This will provide a sufficient number of ensembles to compute statistics such as mean velocity, rms velocity, the full Reynolds-stress tensor, and two-point correlations in the streamwise and wall-normal flow directions. The results will be compared to hot-wire measurements already obtained to document the equilibrium turbulent boundary layer. In addition, they will serve as a baseline to which comparisons can be made of measurements for the non-equilibrium case.

Measurements in the x-z plane will be taken at the same Re_θ values outlined in the above section. These measurements will be taken on the side of the cylinder at various wall-normal locations spanning the logarithmic region of the boundary layer. A schematic of the optics used to create and position the light sheet are shown in Figure 8. They will provide an instantaneous picture of the spanwise structure of the flow field in the equilibrium boundary layer as a function of Reynolds number. In addition, any wall-normal variation in the spanwise structure of the boundary layer will be documented. As before, statistics such as mean velocity, rms velocity, Reynolds-stress tensor and two-point correlations in the spanwise direction will be computed. Again the results will serve as a baseline to which comparisons can be made of similar measurements in the non-equilibrium boundary layer.

All measurements to date were made with the light sheet in the x-y plane of the flow. Figures 9 and 10 depict the instantaneous velocity components (u,v,w) of four randomly selected PIV realizations. A constant convection velocity of $0.9U_\infty$ has been subtracted from the u-component of velocity to better show the turbulent fluctuations. The magnitude and direction u-v velocity fluctuations are indicated by the length and direction of the vectors. The w-component of the turbulent velocity fluctuations is given by the contour color where

the color bar indicates both the magnitude and direction of the fluctuation. As observed in earlier work by Adrian and co-workers, there is an internal layer character close to the wall. This internal layer, seen as a region of uniformly low momentum that extends from the wall up to about 20mm, is capped by a collection of several intense spanwise vortices. Also, it is immediately clear that the values of the w-component are frequently as large or larger than the streamwise and normal velocity component fluctuations.

Although the funding for this investigation under this contract has ended, Steve Gravante is planning on continuing his Ph.D. work on the experimental investigation of the flow associated with the non-equilibrium effects introduced by the rotating segment of the cylinder. These experiments are planned for the Spring and Summer of 1998.

References

Anderson, S. D., and Eaton, J. K., "Reynolds Stress Development in Pressure-Driven Three-Dimensional Turbulent Boundary Layers," *Journal of Fluid Mechanics,* Vol. 202, pp. 263-294, 1989.

Bradshaw, P., "Calculation of Three-Dimensional Boundary Layer Flows," *Journal of Fluid Mechanics*, Vol. 46, part 3, pp. 417-445, 1971.

Driver, D. M., and Johnston, J. P., "Experimental Study of a Three-Dimensional Shear-Driven Turbulent Boundary Layer with Streamwise Adverse Pressure Gradient," *NASA TM 102211*, May 1990.

Driver, D. M., and Hebbar, S. K., "Experimental Study of a Three-Dimensional, Shear-Driven Turbulent Boundary Layer," *AIAA Journal*, Vol. 25, No. 1, pp. 35-42, 1987.

Fernholz, H. H., and Vagt, J. D., "Turbulence Measurements in an Adverse Pressure Gradient Three-Dimensional Turbulent Boundary Layer a Long a Circular Cylinder," *Journal of Fluid Mechanics,* Vol. 111, 233-269, 1981.

Furuya, Y., Nakamura, I., and Kawachi, H., "The Experiment on the Skewed Boundary Layer on a Rotating Body," *Bulletin of Japan Society of Mechanical Engineers*, Vol. 9, p. 702, 1966.

Higuchi, H., and Rubesin, M. W, "Behavior of a Turbulent Boundary Layer Subjected to Sudden Transverse Strain," *AIAA Journal*, Vol. 17, No. 9, pp. 931-941, 1979.

Hites, M.H. (1997). "Scaling of High-Reynolds Number Turbulent Boundary Layers In the National Diagnostic Facility", Ph.D. Thesis. Illinois Institute of Technology, Chicago, IL

Johnston, J. P., "Experimental Studies in Three-Dimensional Turbulent Boundary Layers," *Stanford University Thermosciences Div. Rep. MD-34*, 1976.

Kiwan, S. M. (1995). "Computations of a Shear Drive Three-Dimensional Turbulent Boundary Layer", Ph.D. Thesis. Illinois Institute of Technology, Chicago, IL

Lohmann, R. P., "The Response of a Developed Turbulent Boundary Layer to Local Transverse Surface Motion," *Transactions of ASME, Journal of Fluids Engineering*, Vol. 98, pp. 354-363, 1976.

Purtell, L. P., "Turbulence in Complex Flows: a Selected Review," *AIAA Paper 92-0435*, Presented at 30th Aerospace Sciences Meeting, Reno, Nivada, January 1992.

Schwarz, W. R., and Bradshaw, P., "Turbulence Structural Changes for a Three-Dimensional Turbulent Boundary Layer in a 30° Bend," *Journal of Fluid Mechanics,* Vol. 272, pp. 183-209, 1994.

Speziale, C. G., "On Nonlinear k-l and k-ε Models of Turbulence," *Journal Fluid Mechanics*, Vol. 178, pp. 459-475, 1987.

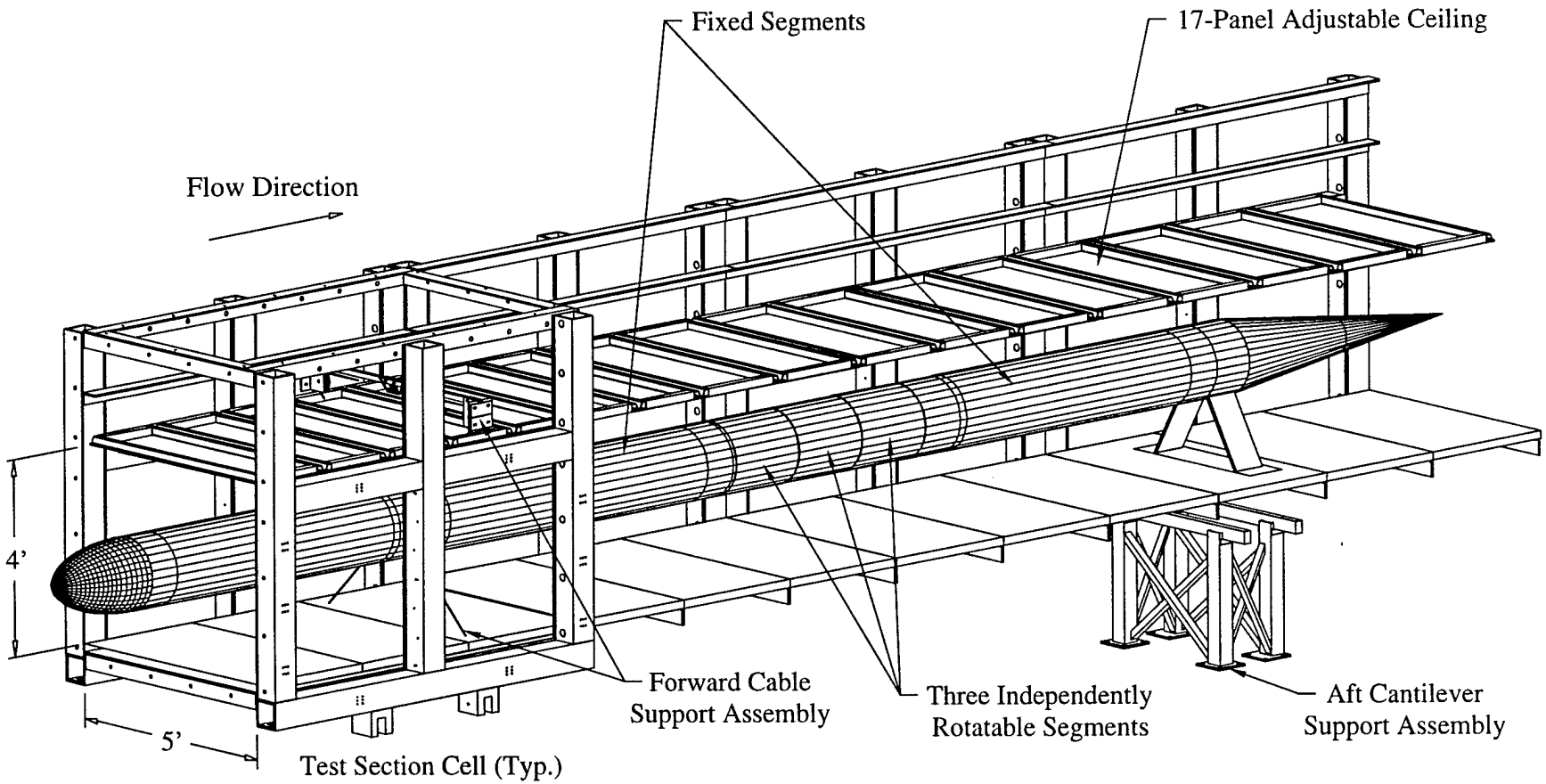

Figure 1 A Three-Dimensional View of the Rotating Cylinder Model Installed within The National Diagnostic Facility

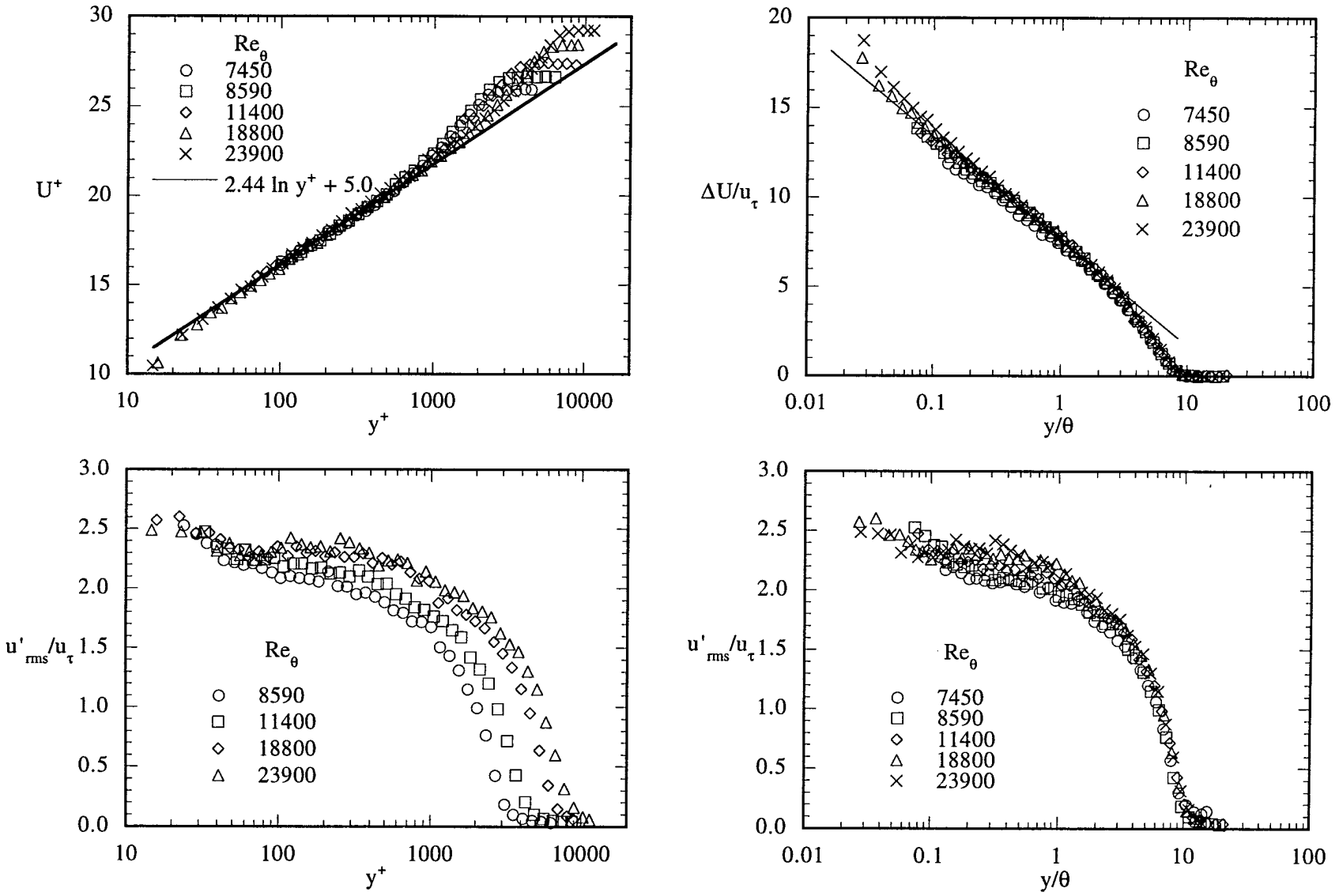

Figure 2. Scaling of the mean velocity profile (top, left) and rms velocity (bottom, left) with inner variables, and scaling of the mean velocity profile (top, right) and rms velocity (bottom, right) with outer variables.

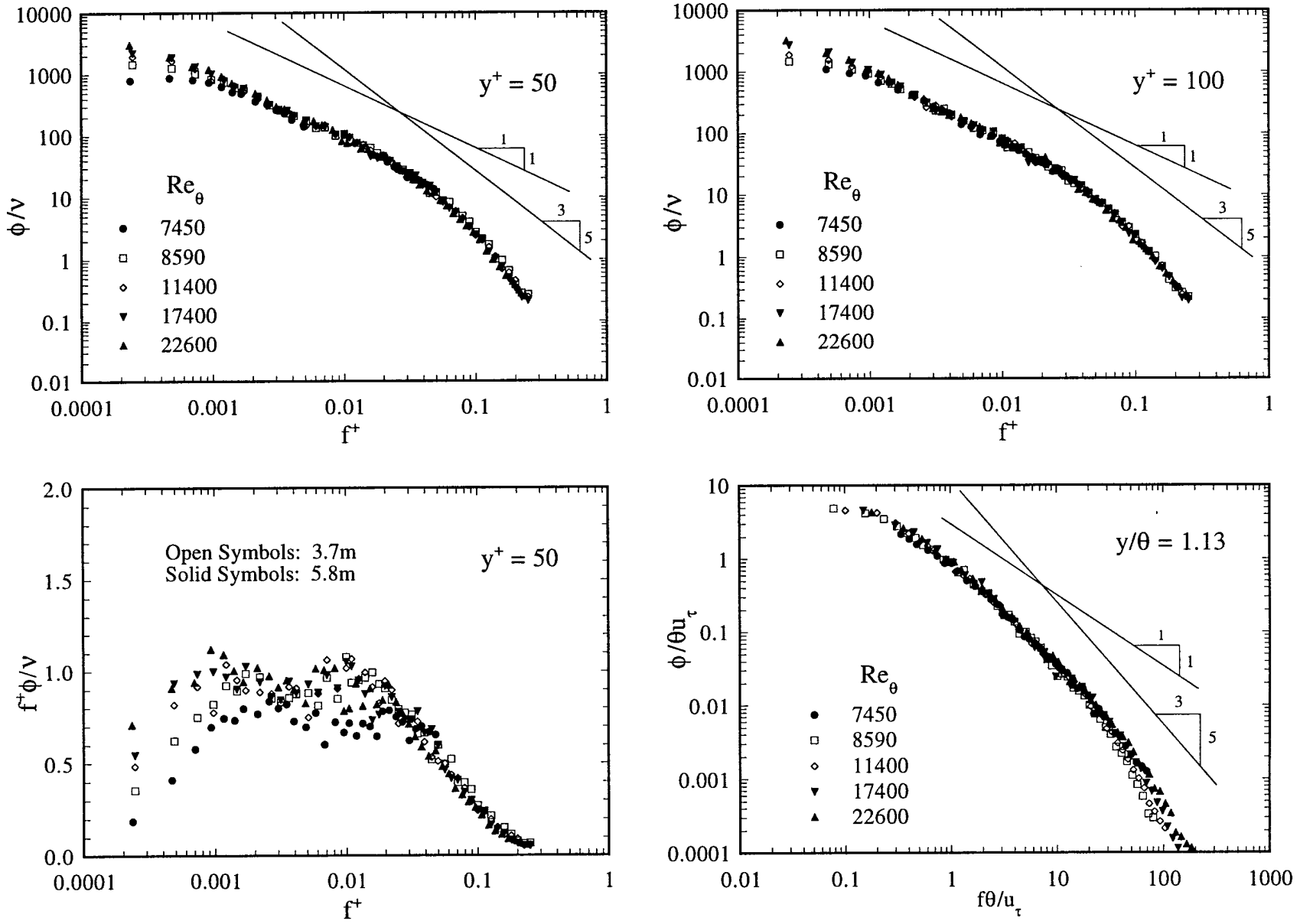

Figure 3. Scaling of the streamwise velocity spectra with inner variables at $y^+ = 50$ (left), and at $y^+ = 100$ (top, right), and scaling of the streamwise velocity spectra with outer variables at $y/\theta = 1.13$.

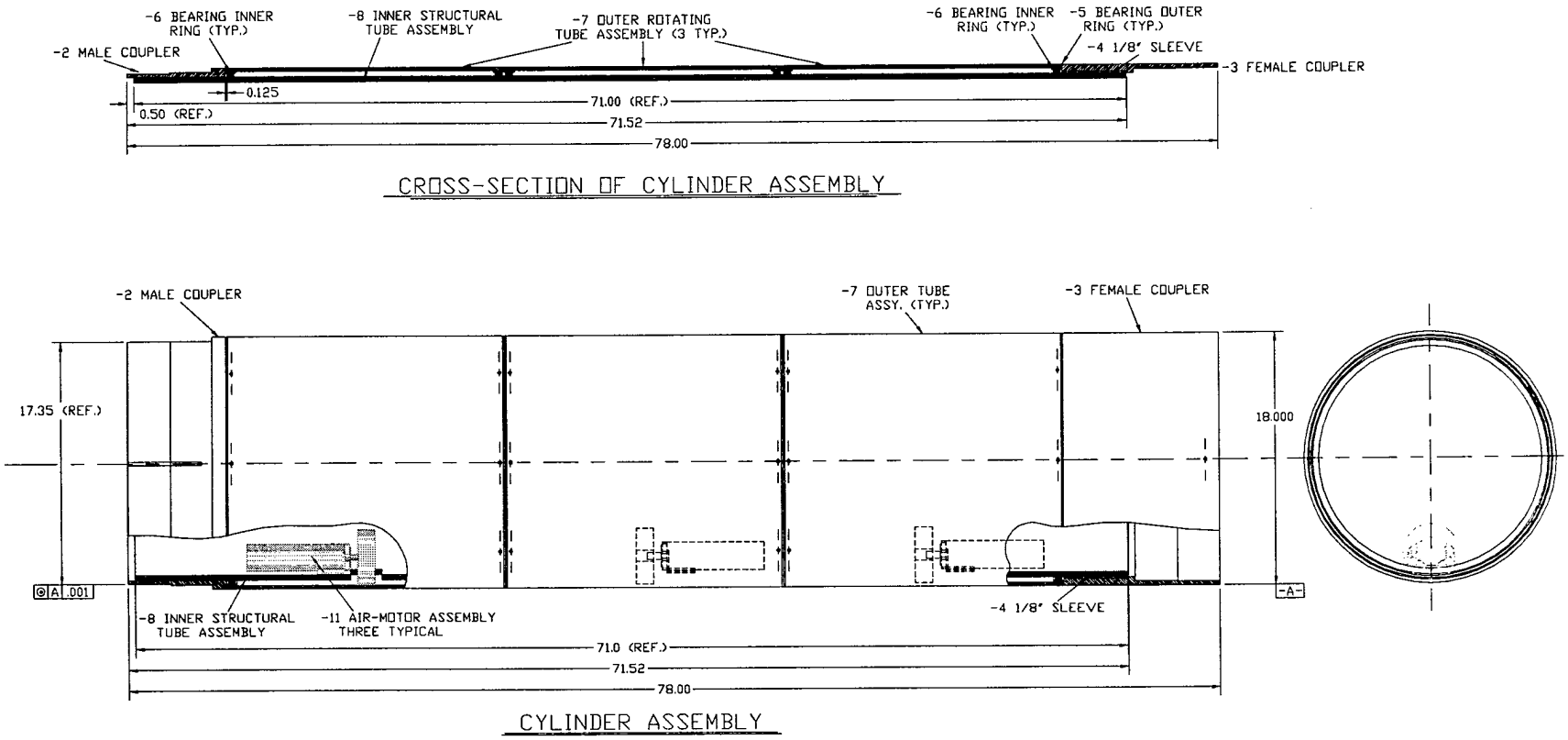

Figure 4 The Rotating Cylinder Section Assembly with Motors

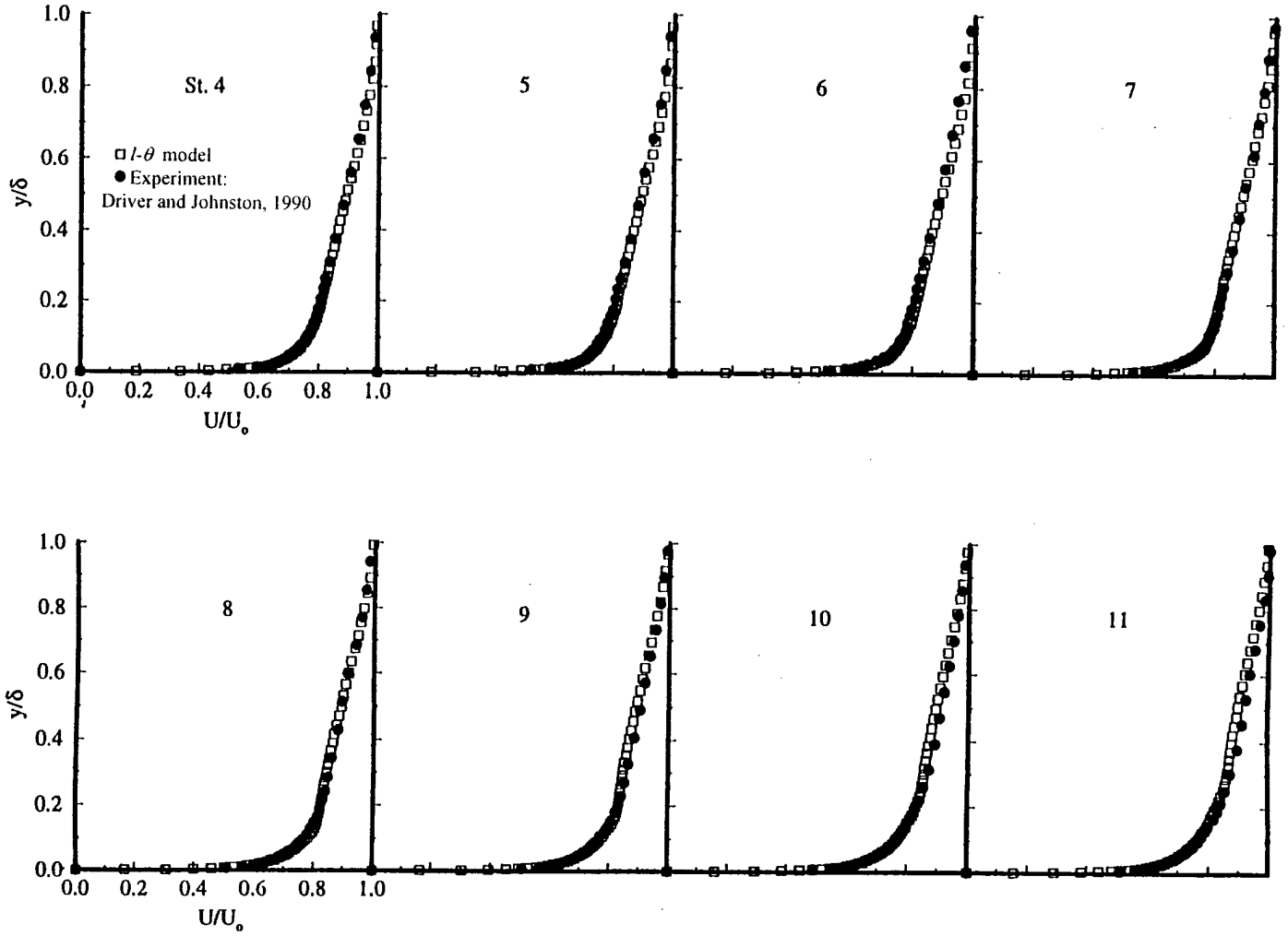

Figure 5. Computational and Experimental Axial Velocity Profiles along the Stationary Segment.

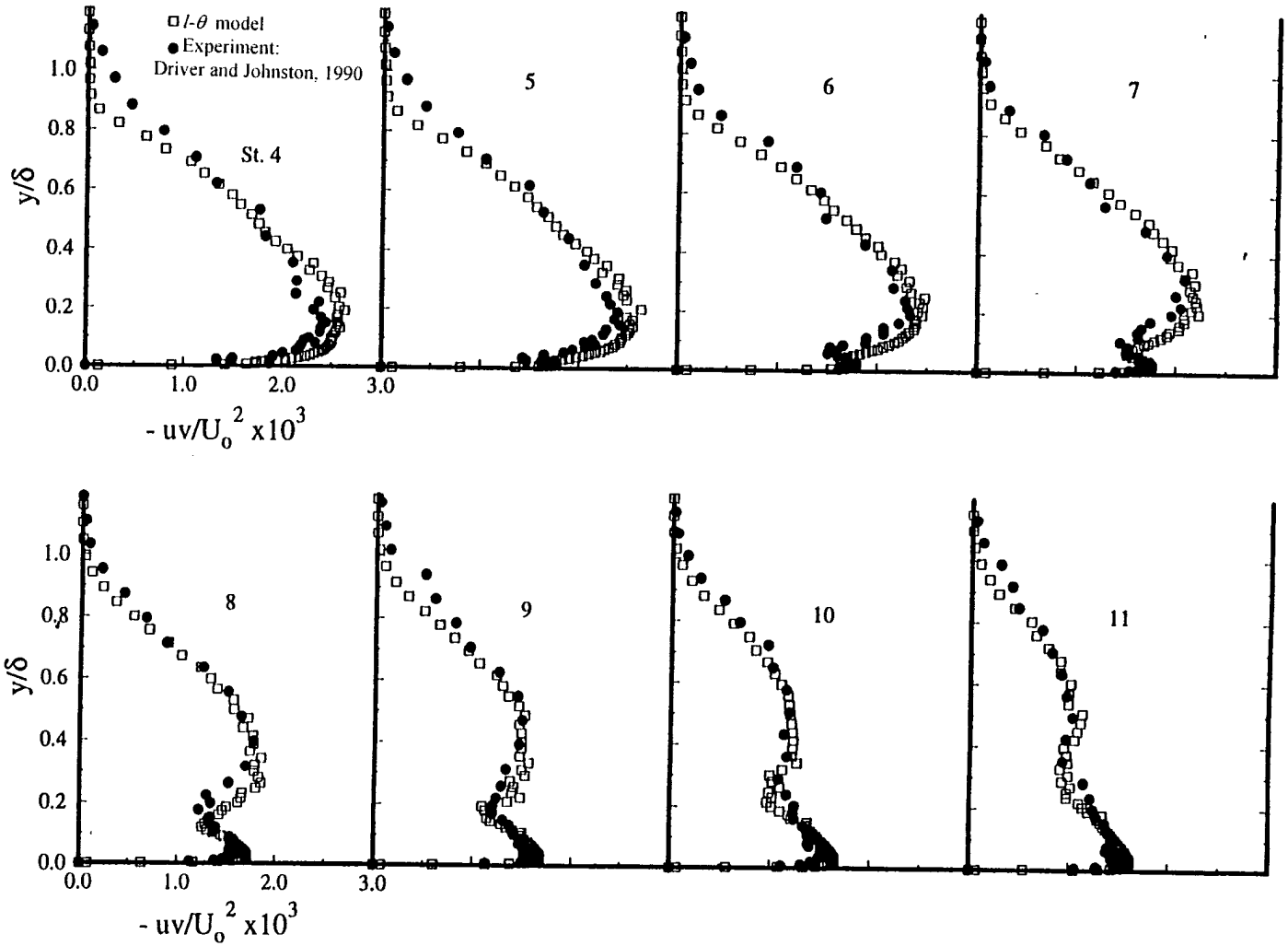

Figure 6. Computational and Experimental Axial Reynolds Stress Profiles along the Stationary Segment.

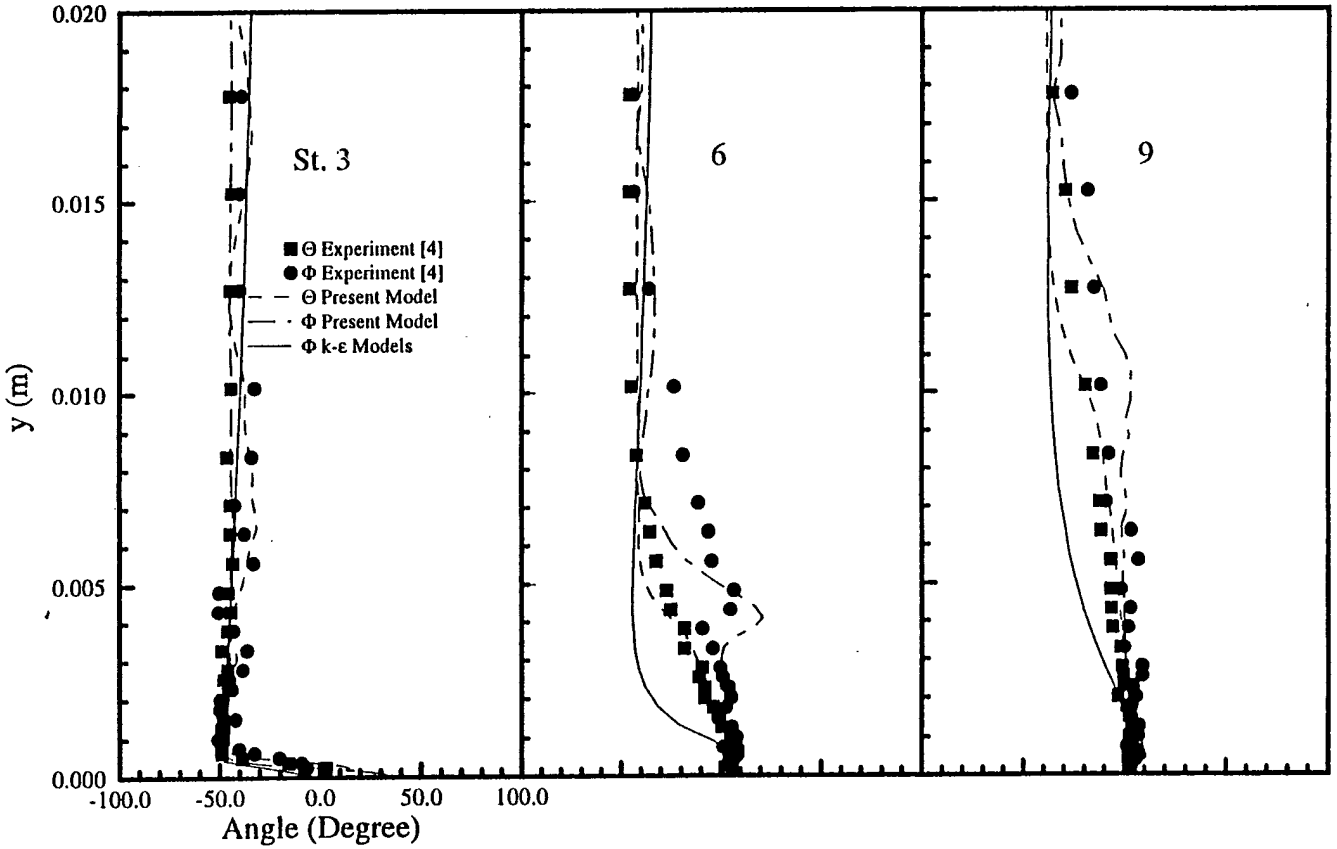

Figure 7. Comparison of the Computational Values of the Stress and Strain Angles at Three Stations over the Stationary Cylinder with the Measurements of Driver and Johnston (1990).

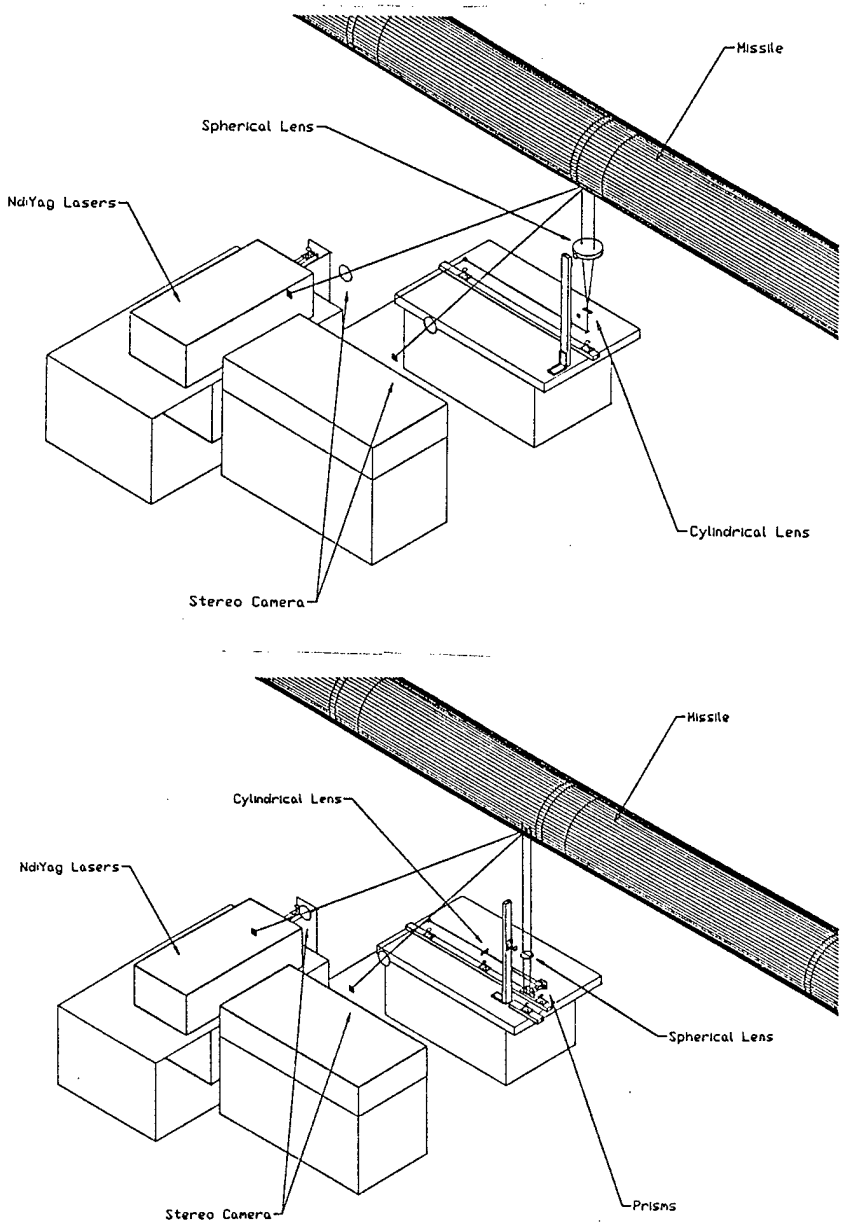

Figure 8. A Schematic of the Optics setup for the x-y plane (top) and x-z plane (bottom) measurements.

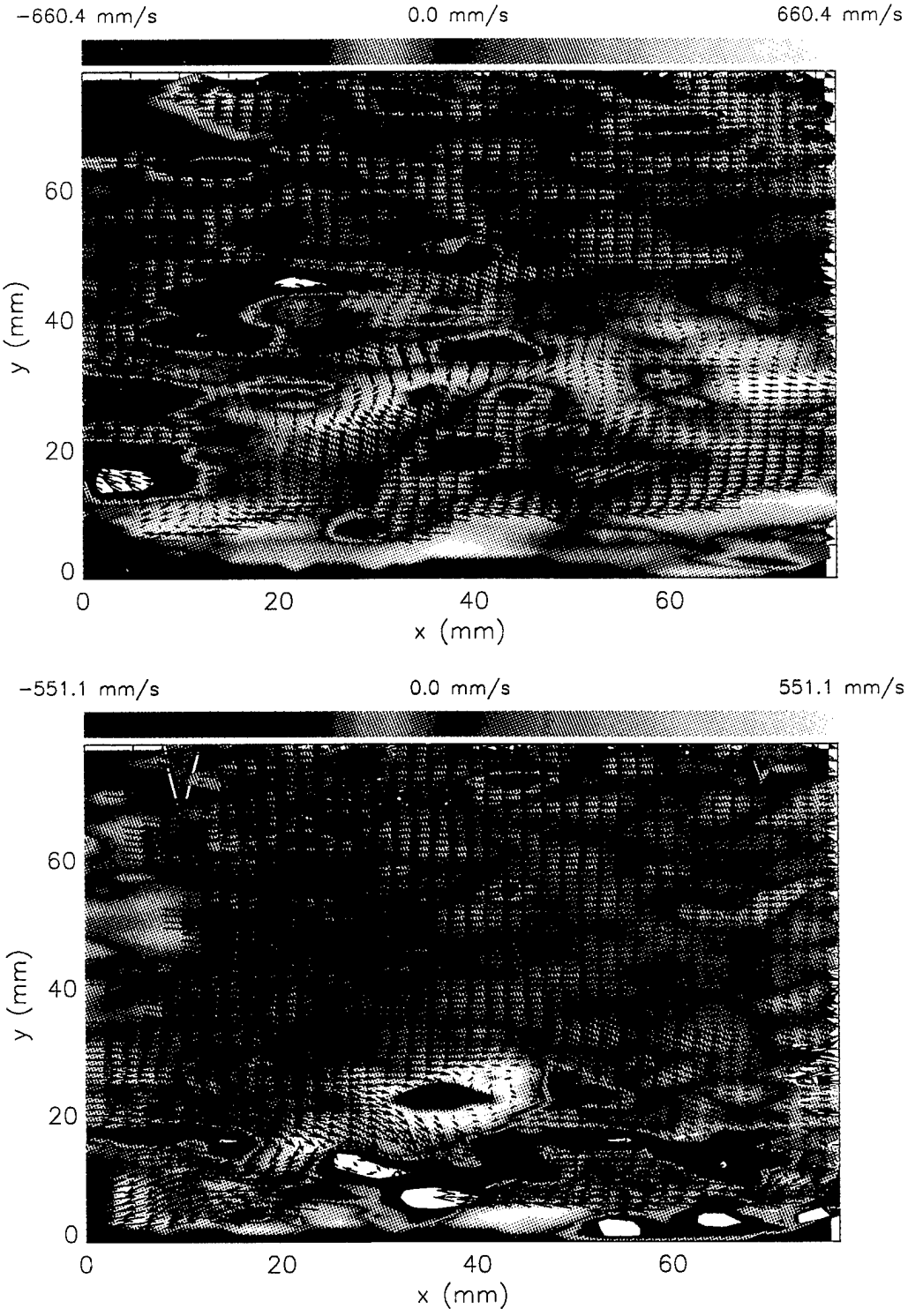

Figure 9 Instantaneous u, v, and w velocity fluctuations.

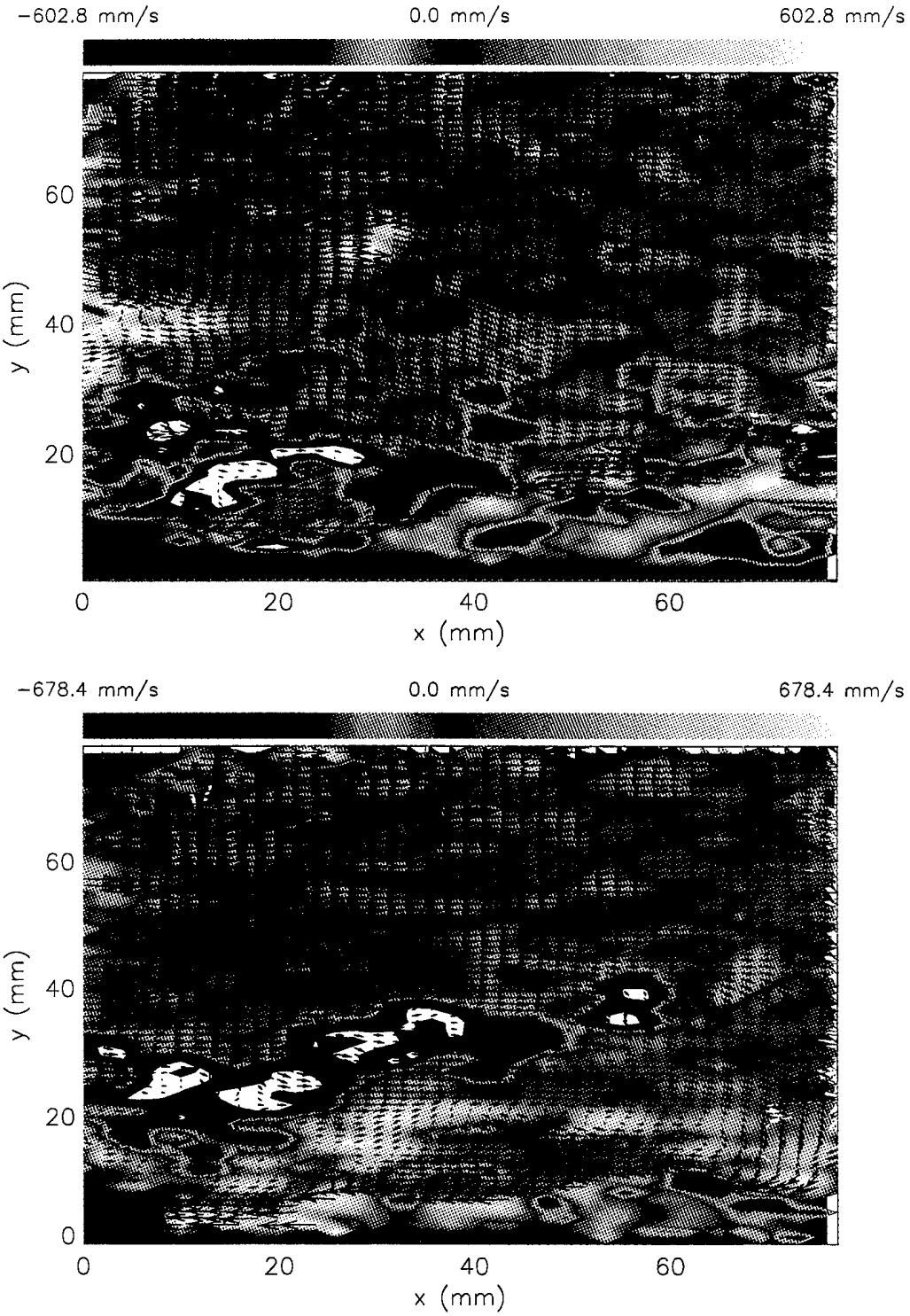

Figure 10 Instantaneous u, v, and w velocity fluctuations.